The Evolution of Baryonic Mass Function of Galaxies to $z = 3$

Zhizheng Pan[1,2] , Yingjie Peng[3], Xianzhong Zheng[1,2], Jing Wang[3], and Xu Kong[2,4]

[1] Purple Mountain Observatory, Chinese Academy of Sciences, 10 Yuan Hua Road, Nanjing, Jiangsu 210033, People's Republic of China; panzz@pmo.ac.cn, xzzheng@pmo.ac.cn

[2] School of Astronomy and Space Sciences, University of Science and Technology of China, Hefei 230026, People's Republic of China; xkong@ustc.edu.cn

[3] Kavli Institute for Astronomy and Astrophysics, Peking University, Yi He Yuan Lu 5, Hai Dian District, Beijing 100871, People's Republic of China

[4] CAS Key Laboratory for Research in Galaxies and Cosmology, Department of Astronomy, University of Science and Technology of China, Hefei, Anhui 230026, People's Republic of China

Abstract

We combine the published stellar mass function (SMF) and gas scaling relations to explore the baryonic (stellar plus cold gas) mass function (BMF) of galaxies to redshift $z = 3$. We find evidence that at $\log(M_{\rm baryon}/M_\odot) > 11.3$, the BMF has evolved little since $z \sim 2.2$. With the evolution of BMF and SMF, we investigate the baryon net accretion rate ($\dot{\rho}_{\rm baryon}$) and stellar mass growth rate ($\dot{\rho}_{\rm star}$) for the galaxy population of $\log(M_{\rm star}/M_\odot) > 10$. The ratio between these two quantities, $\dot{\rho}_{\rm baryon}/\dot{\rho}_{\rm star}$, decreases from $\dot{\rho}_{\rm baryon}/\dot{\rho}_{\rm star} \sim 2$ at $z \sim 2.5$ to $\dot{\rho}_{\rm baryon}/\dot{\rho}_{\rm star} < 0.5$ at $z \sim 0.5$, suggesting that massive galaxies are transforming from the "accretion-dominated" phase to the "depletion-dominated" phase from high-z to low-z. The transition of these two phases occurs at $z \sim 1.5$, which is consistent with the onset redshift of the decline of cosmic star formation rate density (CSFD). This provides evidence to support the idea that the decline of CSFD since $z \sim 1.5$ mainly results from the decline of baryon net accretion rate and star formation quenching in galaxies.

Unified Astronomy Thesaurus concepts: Galaxy evolution (594); Galaxy quenching (2040)

1. Introduction

The distribution of baryonic (stellar plus cold gas) mass of galaxies is of fundamental importance for studying the assembly of galaxies over cosmic time. The first attempt at studying the baryonic mass function (BMF) of galaxies was done by Bell et al. (2003), who found that the local BMF is almost identical to the stellar mass function (SMF) at the high-mass end. This is straightforward to interpret since the baryon content of local massive galaxies has been dominated by stars. In the low-mass regime, the BMF has a similar low-end slope as the SMF. Similar features are also found by later studies that are based on different galaxy samples (Papastergis et al. 2012; Eckert et al. 2016). To date, the investigation of BMF is limited to the local universe.

With the advent of deep surveys in the past two decades, the investigation of SMF has now been pushed out to redshift $z = 8$ (Ilbert et al. 2010, 2013; Muzzin et al. 2013; Tomczak et al. 2014; Song et al. 2016; Davidzon et al. 2017). In the meantime, new observations have facilitated the study of gas properties of high-redshift galaxies in greater detail. Generally, galaxies tend to have a higher gas fraction toward higher redshifts (Tacconi et al. 2010, 2013; Gowardhan et al. 2019). Specifically, Tacconi et al. (2013) found that at $z \sim 2.2$, the ratio between gas mass and total baryonic mass, $f_{\rm gas} = M_{\rm gas}/(M_{\rm gas} + M_{\rm star})$, is around 50% for a galaxy with $\log(M_{\rm star}/M_\odot) = 11.0$. Given this, stellar mass maybe no longer dominate the baryonic budget of a galaxy even at the high-mass end in the early universe.

In this Letter, we aim to combine the newly published SMF of Davidzon et al. (2017) and the gas scaling relations of Tacconi et al. (2018) to push the investigation of BMF to $z = 3$. In Section 2, we introduce the methodology used in this work. In Section 3, we present the derived BMF. In Section 4, we compare the baryon net accretion rate and stellar mass growth rate for galaxies with $\log(M_{\rm star}/M_\odot) > 10$. A short

summary and discussion are presented in Section 5. Throughout this Letter, we adopt a concordance ΛCDM cosmology with $\Omega_{\rm m} = 0.3$, $\Omega_\Lambda = 0.7$, $H_0 = 70\,{\rm km\,s^{-1}\,Mpc^{-1}}$ and a Chabrier (2003) initial mass function. $M_{\rm gas}$ of this work refers to the gas mass of atomic plus molecular hydrogen in the interstellar medium (ISM), which have included a correction of 1.36 to account for helium.

2. Methodology

Galaxies with the same $M_{\rm star}$ may have different $M_{\rm gas}$. Given this, galaxies of similar $M_{\rm star}$ could exhibit a broad distribution in the $M_{\rm star} + M_{\rm gas}$ (hereafter $M_{\rm baryon}$) space. For galaxies within each $M_{\rm star}$ bin, once their $M_{\rm baryon}$ distribution is determined, then at a fixed baryonic mass of $M_{\rm baryon}$, the number density of galaxies can be derived using the following equation:

$$\Phi(M_{\rm baryon}) = \sum_{i=1}^{N} \Phi(M_{\rm baryon}|M_i), \qquad (1)$$

where $\Phi(M_{\rm baryon}|M_i)$ is the number density of galaxies with a baryonic mass of $M_{\rm baryon}$ in the stellar mass M_i bin.

Galaxies are generally categorized into two populations at least out to a redshift $z = 3$–4, which are known as star-forming galaxies (SFGs) and quiescent galaxies (QGs; Strateva et al. 2001; Williams et al. 2009; Davidzon et al. 2017). SFGs follow a relatively tight star formation rate (SFR)–$M_{\rm star}$ relation (the star formation main sequence) up to redshift $z = 5$–6 (Noeske et al. 2007; Speagle et al. 2014). At a given $M_{\rm star}$, SFGs typically have a dispersion of $\sigma_{\rm MS} \sim 0.3$ dex in their SFRs (Guo et al. 2013; Speagle et al. 2014). By contrast, QGs generally have SFRs that are 1–2 dex lower than SFGs. At a given $M_{\rm star}$, QGs are ~ 1 dex lower in gas fraction compared to SFGs (Spilker et al. 2018; Bezanson et al. 2019). In this work, we neglect the contribution of gas mass from QGs to the

baryonic budget, i.e., the baryonic mass of a QG is assumed to be $M_{baryon,QG} = M_{star,QG}$. In this case, the BMF of QGs has a same form as the SMF.

For SFGs, the gas content should be considered, i.e., $M_{baryon,SFG} = M_{star,SFG} + M_{gas,SFG}$. The cold gas component of an SFG consists of molecular and atomic hydrogen (H_2 and $H I$). Thanks to the increasing size of galaxies with CO or far-infrared observations at high redshifts, the properties of molecular gas content of SFGs have been extensively investigated in recent years. In Tacconi et al. (2018), the authors collected the largest sample to date to investigate the molecular gas content of galaxies in relations to their locations on the main sequence and redshift. According to Tacconi et al. (2018), at a given M_{star}, the molecular gas mass of SFGs (M_{H2}) has a dispersion of $\sigma = 0.52 \times \sigma_{MS} \sim 0.15$ dex in the log space when inserting $\sigma_{MS} = 0.3$ dex.

The $H I$ content of SFGs can not be studied directly beyond redshift $z = 0.4$ due to the present observational limit. Although the evolution of cosmic $H I$ density ($\Omega_{H I}$) at $z < 5$ has now been constrained using the observations of damped Lyα systems (DLAs; see Hu et al. 2019 and references therein), it is still difficult to use these observations to infer the $H I$ content in the ISM, due to the fact that $\Omega_{H I}$ inferred from DLAs contains the neutral gas that residing in the ISM and circumgalactic medium (CGM). Theoretical studies have suggested that at $z > 1.75$, the majority of $\Omega_{H I}$ is contributed by the CGM, rather than the ISM (van de Voort et al. 2012; Lagos et al. 2018). Recently, Popping et al. (2015) used an indirect technique to infer the evolution of cold ISM from $z = 3$ to $z = 0.5$, finding that at fixed M_{star}, the atomic hydrogen component in the ISM shows no redshift dependence. In this work, we thus use a redshift-independent M_{star}–$M_{H I}$ relation to infer $M_{H I}$ in galaxies.

In the local universe, Saintonge et al. (2016) found that both $M_{H I}$ and M_{H2} are dependent on the location of SFGs on the main sequence (MS; ΔMS), in the sense that galaxies above/below the ridge line of the main sequence have elevated/suppressed $M_{H I}$ and M_{H2} compared to mean values. However, the $M_{H I}/M_{H2}$ mass ratio is insensitive to ΔMS. To account for $M_{H I}$, in this work we express the total gas mass M_{gas} as

$$M_{gas} = (1 + f)M_{H2}, \tag{2}$$

where $f = M_{H I}/M_{H2}$. At $z > 0$, we assume that f is also insensitive to ΔMS as found in the local universe. To derive M_{gas}, one needs to quantify M_{H2} and the f factor. In this work, M_{H2} is derived by utilizing the scaling relation of Tacconi et al. (2018). On the other hand, f is calculated using the M_{star}–$M_{H I}$ relation of Pan et al. (2019), assuming that this relation does not evolve during $z = [0, 3]$. As such, in each redshift bin, f can be determined by

$$f = M_{H I}/M_{H2}(\Delta MS = 0), \tag{3}$$

where $M_{H I}$ at $\Delta MS = 0$ is from Equation (4) of Pan et al. (2019).

We divide galaxies with a mass bin of $\Delta \log M_{star} = 0.1$ dex and use the Monte Carlo method to derive the M_{baryon} distribution of galaxies in each bin. At a given M_{star} bin, we first generated a sample of N_{gal} galaxies and assigned an M_{gas} to each of them. The assigned M_{gas} peaks at the value set by Equation (2), with a dispersion of $\sigma \sim 0.15$ dex. By doing so, the M_{baryon} distribution of these N_{gal} galaxies can be determined directly. In Figure 1, we show an example of the M_{gas} and
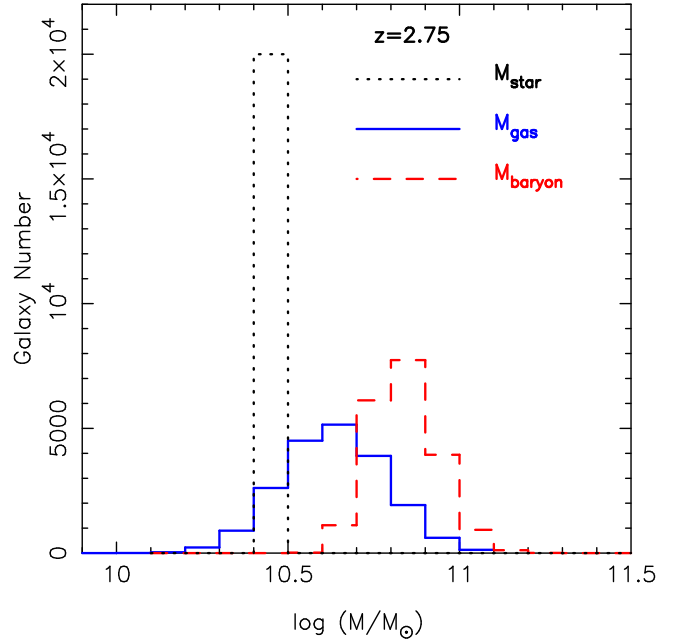

Figure 1. Example of our sampling at $z = 2.75$ for the star-forming galaxies with $\log (M_{star}/M_\odot) = 10.4$. The M_{star}, M_{gas}, and M_{baryon} distributions are shown in different lines.

M_{baryon} distribution of our generated galaxies for the $\log(M_{star}/M_\odot) = 10.4$ bin at $z = 2.75$. The M_{baryon} distribution of these N_{gal} galaxies is then scaled to match the SMF by multiplying a factor of $\Phi(M_{star,SFG})/N_{gal}$, where $\Phi(M_{star,SFG})$ is the number density of SFGs in that M_{star} bin, which is drawn from the measured SMF. Finally, by summing up the SMF-scaled M_{baryon} distributions for each M_{star} bin, we derive the BMF for SFGs, as illustrated in Equation (1). In this work, we use a sufficiently large galaxy number of $N_{gal} = 20000$. Our result is not changed if we choose a larger N_{gal}.

The BMF of the global galaxy population is then derived by combing the BMF of SFGs and QGs, where the BMF of QGs has the same form as their SMF as assumed above. In this work we only focus on galaxies with stellar mass greater than $\log(M_{star}/M_\odot) = 10.0$, since the gas scaling relation of Tacconi et al. (2018) is constructed based on galaxies primarily located in this mass regime.

3. The Baryonic Mass Function

The SMF used in this work is from Davidzon et al. (2017), which is based on the latest data set of the Cosmic Evolution Survey (COSMOS; Scoville et al. 2007). At each redshift, Davidzon et al. (2017) used the NUV $-r$ versus $r - J$ diagram to classify galaxies into SFGs and QGs, and measured their SMF separately. At redshift $z = 3$, the SMF is mass completed to $\log(M_{star}/M_\odot) = 9.0$, which is sufficiently deep for our study. In the top left and top right panels of Figure 2, we show the SMF and gas mass function (GMF) for the galaxy population of $\log(M_{star}/M_\odot) > 10.0$. At $z < 1$, it can be seen that the SMF evolves little, while the GMF still has a significant evolution. The bottom left panel presents our derived BMF. In the low-mass regime, the BMF is highly incomplete because we do not include the galaxy population of $\log(M_{star}/M_\odot) < 10.0$. At each redshift, we arbitrarily define a limited mass (M_{limit}) below which the effect of incompleteness
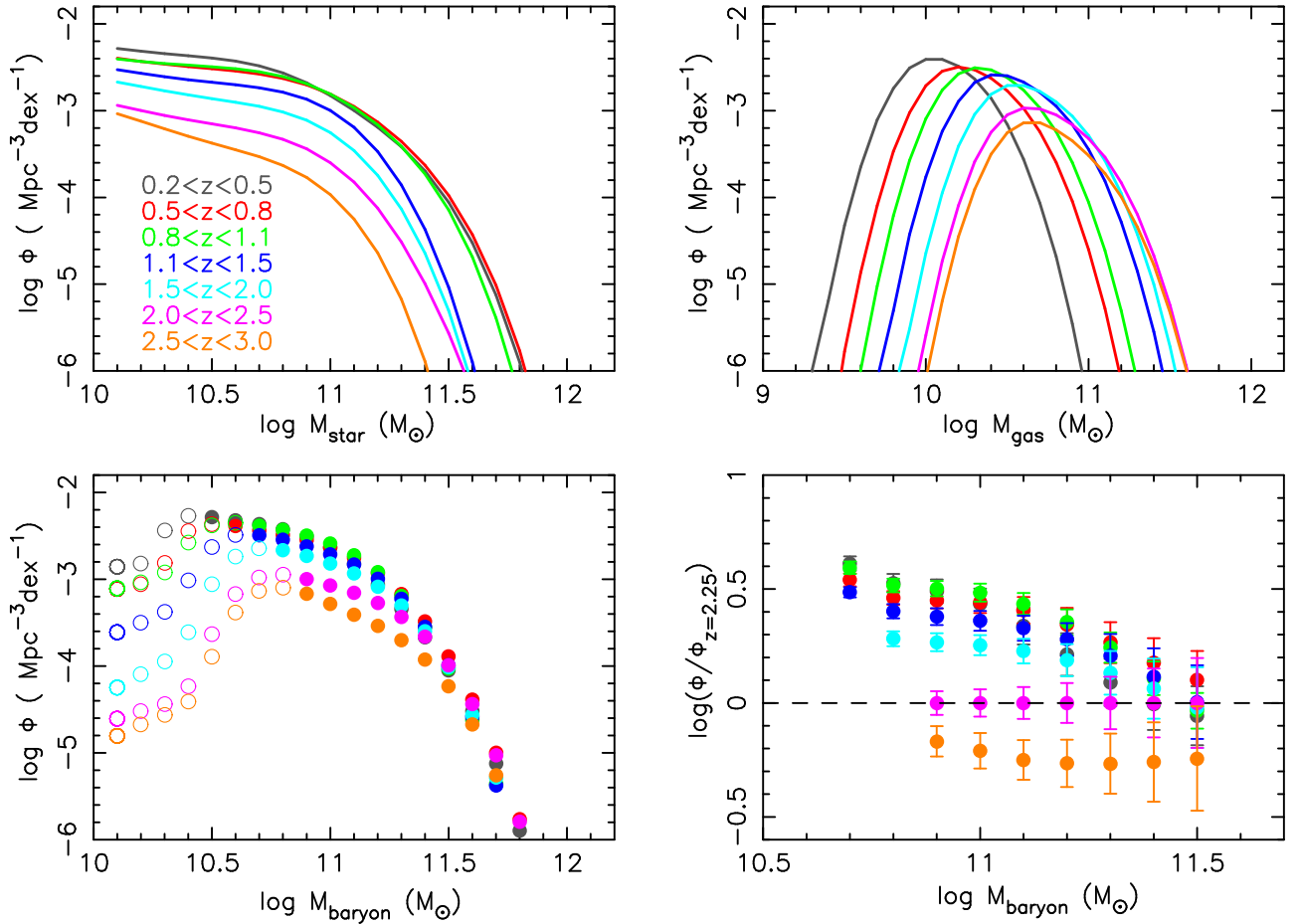
Figure 2. Top left: the stellar mass function of Davidzon et al. (2017). Top right: the M_{gas} distribution for the $\log(M_{star}/M_\odot) > 10.0$ population. Bottom left: the baryonic mass function of galaxies. Solid and open symbols indicate the galaxies with $M_{baryon} \geqslant M_{limit}$ and $M_{baryon} < M_{limit}$, respectively. Bottom right: growth of the baryonic mass function relative to the $z = 2.25$ redshift bin. We only show the result for the $M_{baryon} > M_{limit}$ galaxies. The error bars are derived by including the 1σ Poisson uncertainty of the SMF and ± 0.1 dex uncertainty in M_{gas} estimation. In all panels, galaxies of different redshift bins are indicated by different colors.

Table 1
Schechter Parameters of the Baryonic Mass Function

Redshift	Mass Limit $\log M_{limit}(h_{70}^{-2}\,M_\odot)$	α	$\phi_\star$ $10^{-3}h_{70}^3\,\mathrm{Mpc}^{-3}$	$M_\star$ $\log M(h_{70}^{-2}M_\odot)$
$0.2 < z \leqslant 0.5$	10.5	$-0.42^{+0.05}_{-0.05}$	$5.19^{+0.06}_{-0.06}$	$10.68^{+0.01}_{-0.01}$
$0.5 < z \leqslant 0.8$	10.6	$-0.77^{+0.05}_{-0.04}$	$3.45^{+0.14}_{-0.14}$	$10.88^{+0.02}_{-0.02}$
$0.8 < z \leqslant 1.1$	10.6	$-0.41^{+0.05}_{-0.04}$	$4.64^{+0.05}_{-0.05}$	$10.75^{+0.01}_{-0.01}$
$1.1 < z \leqslant 1.5$	10.7	$-0.73^{+0.05}_{-0.04}$	$3.09^{+0.09}_{-0.08}$	$10.86^{+0.02}_{-0.02}$
$1.5 < z \leqslant 2.0$	10.8	$-0.60^{+0.05}_{-0.04}$	$2.38^{+0.05}_{-0.05}$	$10.85^{+0.01}_{-0.01}$
$2.0 < z \leqslant 2.5$	10.9	$-0.59^{+0.09}_{-0.08}$	$1.13^{+0.04}_{-0.04}$	$10.93^{+0.03}_{-0.03}$
$2.5 < z \leqslant 3.0$	10.9	$-1.19^{+0.09}_{-0.09}$	$0.55^{+0.06}_{-0.06}$	$11.04^{+0.05}_{-0.05}$

becomes important, where $M_{limit} = M_{peak} + 0.1$.[5] At $M_{baryon} > M_{limit}$, we fit the BMF with a single Schechter function (Schechter 1976). The M_{limit} and best-fit Schechter parameters are summarized in Table 1.

Compared to the SMF, a most remarkable feature of the BMF is that at $\log(M_{baryon}/M_\odot) > 11.3$, the BMF has evolved little since $z \sim 2.2$. Note that we do not account for the uncertainty of SMF in Figure 3. At very high masses, the BMF has a relatively large uncertainty, which is mainly propagated from the SMF. For the SMF of Davidzon et al. (2017), the typical uncertainty is around ± 0.1 dex at $\log(M_{star}/M_\odot) = 11.0$ and ± 0.4 dex at $\log(M_{star}/M_\odot) = 11.5$, respectively. In the bottom right panel, we show the evolution of BMF at $M_{baryon} > M_{limit}$ after accounting for the uncertainty of SMF. We also include a ± 0.1 dex uncertainty in the M_{H2} estimation as suggested by Tacconi et al. (2018). After accounting for these uncertainties, our finding still holds, suggesting that the baryon assembly is close to completion at the high-mass end ever since the peak of cosmic star formation.

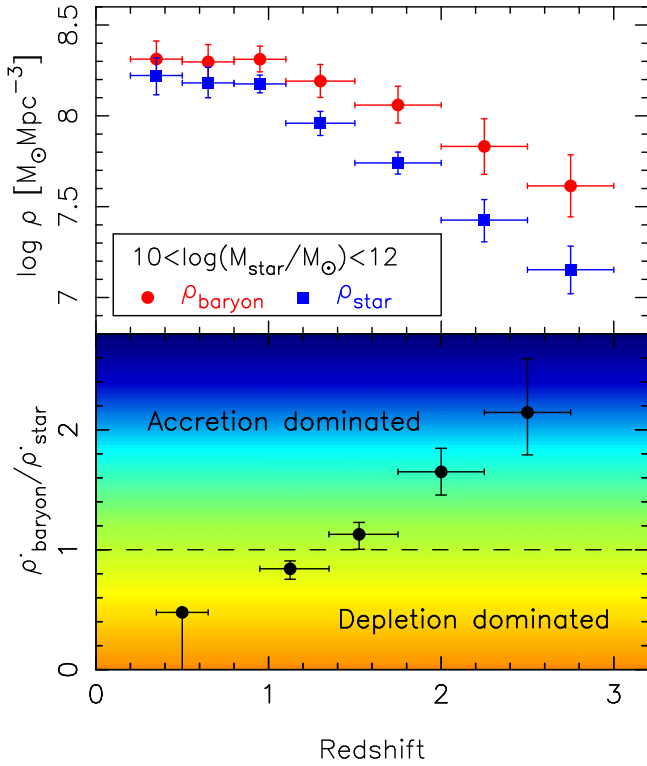[5] M_{peak} is the baryonic mass at which the number density of galaxies reaches the peak value.

Figure 3. Top panel: the growth of stellar mass density ρ_{star} and baryonic mass density ρ_{baryon} for galaxies with $\log(M_{star}/M_{Sun}) > 10.0$. The error bars are derived by considering the 1σ Poisson uncertainty in SMF and the uncertainties of BMF shown in Figure 2. Bottom panel: $\dot{\rho}_{baryon}/\dot{\rho}_{star}$ as a function of redshift.

4. The Baryon Net Accretion Rate and Stellar Mass Growth Rate

Galaxies continuously accrete baryon (from the intergalactic medium (IGM), or mergers) from the surrounding environments and convert the cold gas into stars. With the evolution of BMF and SMF, we can make a direct comparison between baryon net accretion rate[6] and stellar mass growth rate.

By convolving the BMF and SMF with M_{baryon} and M_{star}, respectively, we derive the stellar mass density ρ_{star} and baryonic mass density ρ_{baryon} for the galaxy population of $\log(M_{star}/M_{\odot}) > 10$. The top panel of Figure 3 shows the evolution of ρ_{star} and ρ_{baryon} as a function of redshift. It can be seen that ρ_{star} and ρ_{baryon} increase by a factor of ~ 1 dex ($\times 10$) and ~ 0.7 dex ($\times 5$) from $z = 3$ to $z = 1$, respectively. At $z < 1$, both ρ_{star} and ρ_{baryon} show little evolution. During a specific redshift interval $[z_1, z_2]$, the changing rate of ρ_{star} and ρ_{baryon} can be expressed as

$$\dot{\rho}_{star} = \triangle \rho_{star}/\Delta t = (\rho_{star,z_1} - \rho_{star,z_2})/\Delta t \qquad (4)$$

and

$$\dot{\rho}_{baryon} = \triangle \rho_{baryon}/\Delta t = (\rho_{baryon,z_1} - \rho_{baryon,z_2})/\Delta t, \qquad (5)$$

where $\triangle t$ is the time interval between z_1 and z_2. Hence, at the same redshift interval, $\dot{\rho}_{baryon}/\dot{\rho}_{star} = \Delta\rho_{baryon}/\triangle \rho_{star}$.

The bottom panel of Figure 3 shows $\dot{\rho}_{baryon}/\dot{\rho}_{star}$ as a function of redshift. At $z \sim 2.5$, $\dot{\rho}_{baryon}/\dot{\rho}_{star} \sim 2.0$, indicating that the baryon net accretion rate significantly exceeds the stellar mass growth rate. Assuming that the increase of ρ_{baryon}

and ρ_{star} is primarily due to IGM accretion and stellar mass conversion in galaxies, the global gas density of these galaxies (not for individual) would continuously increase during this epoch. We call this as an "accretion-dominated" phase. $\dot{\rho}_{baryon}/\dot{\rho}_{star}$ decreases at later epochs to a level of $\dot{\rho}_{baryon}/\dot{\rho}_{star} \sim 1.0$ at $z \sim 1.5$. When $\dot{\rho}_{baryon}/\dot{\rho}_{star} < 1.0$, the net-accreted baryon is no longer capable in sustaining stellar mass growth, and the gas reservoir of galaxies are being depleted. At $z \sim 0.5$, $\dot{\rho}_{baryon}/\dot{\rho}_{star} < 0.5$, suggesting that massive galaxies have entered the "depletion-dominated" phase at low redshifts.

It is worthy to emphasize that besides gas accretion and in situ star formation in galaxies, mergers of galaxies with $\log(M_{star}/M_{\odot}) < 10$ will contribute to both ρ_{baryon} and ρ_{star}, hence impacting the $\dot{\rho}_{baryon}/\dot{\rho}_{star}$ ratio.[7] Since the low-mass galaxies typically have a higher gas-to-stellar mass ratio than the massive ones, merging of low-mass galaxies will increase the $\dot{\rho}_{baryon}/\dot{\rho}_{star}$ ratio. Assuming that the influence of low-mass mergers is small, the $\dot{\rho}_{baryon}/\dot{\rho}_{star}$ in Figure 3 largely reflects the relation between gas net accretion rate and stellar mass conversion rate in galaxies.

5. Summary and Discussion

We combine the recently published SMF and the gas scaling relations to explore the evolution of galaxy BMF of galaxies to redshift $z = 3$. We find evidence that at $\log(M_{baryon}/M_{\odot}) > 11.3$, the BMF evolves little since $z \sim 2.2$. By studying the evolution of stellar mass density ρ_{star} and baryonic mass density ρ_{baryon} for the $\log(M_*/M_{\odot}) > 10$ galaxy population, we find that these galaxies transform from the "accretion-dominated" phase to the "depletion-dominated" phase from high-z to low-z, with a transition redshift of $z_{tran} \sim 1.5$.

The robustness of our derived BMF relies on the accuracy of both the SMF measures and M_{gas} estimation. At $z < 3$, the SMF measures (both for SFGs and QGs) from different surveys have reached very good agreement for the mass range of $\log(M_{star}/M_{\odot}) = 10.0$–$11.3$ (Ilbert et al. 2013; Tomczak et al. 2014; Davidzon et al. 2017). We have also tried the SMF drawn from Ilbert et al. (2013) and Tomczak et al. (2014) and found that the change of the BMF is within ± 0.1 dex at $\log(M_{baryon}/M_{\odot}) < 11.3$. At higher masses, the discrepancy increases, which mainly results from cosmic variance. For M_{gas}, Tacconi et al. (2018) stated that the population-average M_{H2} estimation can reach an accuracy of ± 0.1 dex based on their scaling relations. We have considered $\Delta\log(M_{H2}) = 0.1$ dex and found that it contributes ~ 0.03–0.07 dex uncertainty in the BMF at $\log(M_{baryon}/M_{\odot}) < 11.3$. Another source of uncertainty comes from the M_{HI} estimation. In this work we have assumed an unevolved $M_{star} - M_{HI}$ relation at $z < 3$. At fixed M_{star}, if we allow M_{HI} to vary ± 0.5 dex since $z = 3$ with a simple form of $\log M_{HI} = \log M_{HI,z=0} + a \times \log(1 + z)$, this will bring in an uncertainty of ~ 0.0–0.12 dex in the BMF, depending on redshift. So if the $M_{star} - M_{HI}$ relation does not significantly evolve during $z < 3$, our BMF should be robust.

The little evolution of BMF at $\log(M_{baryon}/M_{\odot}) > 11.3$ since $z \sim 2.2$ implies that the baryon assembly is close to completion in these galaxies since then. How should one interpret this phenomenon? At $z < 1$, this is another reflection

---

[6] Net accretion rate = accretion rate−outflow rate.

[7] Mergers between galaxies with $\log(M_{star}/M_{\odot}) > 10$ do not contribute to $\triangle\rho_{star}$ and $\triangle\rho_{baryon}$, thus will not impact the $\dot{\rho}_{baryon}/\dot{\rho}_{star}$ ratio.

of the little evolution of SMF (see Figure 2), since the baryon content of massive galaxies has been dominated by stars. At $z > 1$, there are some interpretations to this phenomenon under the context of the galaxy formation paradigm. One is that the halo masses of these galaxies have exceeded the critical halo mass ($M_c \sim 10^{12} M_\odot$) to support a stable shock, and the halo gas of these galaxies has been shock-heated to prevent efficient cooling (Dekel & Birnboim 2006). The deep potential well of massive halos, on the other hand, is capable of preventing strong gas outflows (Tremonti et al. 2004). The combination of these two effects then naturally results in an extremely low baryon net accretion rate. Alternatively, the low baryon net accretion rate could be resulted from a balance between gas inflows and outflows, without a requirement of a low gas inflow/outflow rate. Some previous works have suggested that high-z massive SFGs could exhibit strong gas outflows due to the strong feedback from supermassive black hole or star formation (Genzel et al. 2014; Yabe et al. 2014). More future work is needed to better understand this phenomenon.

Interestingly, Figure 2 shows that the number density of galaxies with $\log (M_{\rm baryon}/M_\odot) = 11.3$ increases by a factor of 2 (~ 0.3 dex) from $z \sim 2.7$ to $z \sim 2.2$, implying that the baryon net accretion rate in the progenitors of these galaxies must be considerably high during $z = [2.2, 2.7]$. Considering the little evolution of BMF at the massive end since $z \sim 2.2$, some efficient mechanisms are thus required to shut down the baryon net accretion in massive galaxies within a very short timescale (~ 0.5 Gyr). Under the context of the current galaxy formation paradigm, the halo shock-heating scenario and feedback from star formation/the central black hole are potentially responsible for doing this job (Croton et al. 2006; Dekel & Birnboim 2006). Identifying the working mechanism is beyond the scope of this work.

The $\log(M_{\rm star}/M_\odot) > 10$ galaxy population transits from the "accretion-dominated" phase to "depletion-dominated" phase at $z_{\rm tran} \sim 1.5$. Interestingly, $z_{\rm tran}$ is similar to the onset redshift of the decline of the cosmic star formation rate density (CSFD; see the review of Madau & Dickinson 2014). Given that the $\log(M_{\rm star}/M_\odot) > 10$ galaxy population contributes to 40%–50% of the cosmic star formation budget at $z < 3.0$, we suggest that the decline of CSFD since $z \sim 1.5$ is closely related to the decline of baryon net accretion rate in galaxies. This is straightforward to interpret since cold gas accretion is necessary for sustaining star formation (Davé et al. 2011; Lilly et al. 2013; Peng & Maiolino 2014). With the decline of the baryon accretion rate, the star formation rate in galaxies will decrease, which then results in star formation cessation in some galaxies, especially at the high-mass end (Peng et al. 2010; Pan et al. 2016, 2017). The early assembly of baryon content in massive galaxies at $z \sim 2.2$ and the rapid buildup of massive QG population since then support this picture (Ilbert et al. 2013; Muzzin et al. 2013; Tomczak et al. 2014; Davidzon et al. 2017). In summary, our findings support the idea that the decline of CSFD since $z \sim 1.5$ mainly results from the decline of the baryon net accretion rate and star formation quenching in galaxies.

ORCID iDs

Zhizheng Pan ⓘ https://orcid.org/0000-0001-5662-8217
Xu Kong ⓘ https://orcid.org/0000-0002-7660-2273

References

Bell, E. F., McIntosh, D. H., Katz, N., & Weinberg, M. D. 2003, ApJL, 585, L117
Bezanson, R., Spilker, J., Williams, C. C., et al. 2019, ApJL, 873, L19
Chabrier, G. 2003, PASP, 115, 763
Croton, D. J., Springel, V., White, S. D. M., et al. 2006, MNRAS, 365, 11
Davé, R., Finlator, K., & Oppenheimer, B. D. 2011, MNRAS, 416, 1354
Davidzon, I., Ilbert, O., Laigle, C., et al. 2017, A&A, 605, A70
Dekel, A., & Birnboim, Y. 2006, MNRAS, 368, 2
Eckert, K. D., Kannappan, S. J., Stark, D. V., et al. 2016, ApJ, 824, 124
Genzel, R., Förster Schreiber, N. M., Rosario, D., et al. 2014, ApJ, 796, 7
Gowardhan, A., Riechers, D., Pavesi, R., et al. 2019, ApJ, 875, 6
Guo, K., Zheng, X. Z., & Fu, H. 2013, ApJ, 778, 23
Hu, W., Hoppmann, L., Staveley-Smith, L., et al. 2019, MNRAS, 489, 1619
Ilbert, O., McCracken, H. J., Le Fèvre, O., et al. 2013, A&A, 556, A55
Ilbert, O., Salvato, M., Le Floc'h, E., et al. 2010, ApJ, 709, 644
Lagos, C. d. P., Tobar, R. J., Robotham, A. S. G., et al. 2018, MNRAS, 481, 3573
Lilly, S. J., Carollo, C. M., Pipino, A., Renzini, A., & Peng, Y. 2013, ApJ, 772, 119
Madau, P., & Dickinson, M. 2014, ARA&A, 52, 415
Muzzin, A., Marchesini, D., Stefanon, M., et al. 2013, ApJ, 777, 18
Noeske, K. G., Weiner, B. J., Faber, S. M., et al. 2007, ApJL, 660, L43
Pan, Z., Peng, Y., Zheng, X., Wang, J., & Kong, X. 2019, ApJ, 876, 21
Pan, Z., Zheng, X., & Kong, X. 2017, ApJ, 834, 39
Pan, Z., Zheng, X., Lin, W., et al. 2016, ApJ, 819, 91
Papastergis, E., Cattaneo, A., Huang, S., Giovanelli, R., & Haynes, M. P. 2012, ApJ, 759, 138
Peng, Y.-j., Lilly, S. J., Kovač, K., et al. 2010, ApJ, 721, 193
Peng, Y.-j., & Maiolino, R. 2014, MNRAS, 443, 3643
Popping, G., Caputi, K. I., Trager, S. C., et al. 2015, MNRAS, 454, 2258
Saintonge, A., Catinella, B., Cortese, L., et al. 2016, MNRAS, 462, 1749
Schechter, P. 1976, ApJ, 203, 297
Scoville, N., Aussel, H., Brusa, M., et al. 2007, ApJS, 172, 1
Song, M., Finkelstein, S. L., Ashby, M. L. N., et al. 2016, ApJ, 825, 5
Speagle, J. S., Steinhardt, C. L., Capak, P. L., & Silverman, J. D. 2014, ApJS, 214, 15
Spilker, J., Bezanson, R., Barišić, I., et al. 2018, ApJ, 860, 103
Strateva, I., Ivezić, Ž, Knapp, G. R., et al. 2001, AJ, 122, 1861
Tacconi, L. J., Genzel, R., Neri, R., et al. 2010, Natur, 463, 781
Tacconi, L. J., Genzel, R., Saintonge, A., et al. 2018, ApJ, 853, 179
Tacconi, L. J., Neri, R., Genzel, R., et al. 2013, ApJ, 768, 74
Tomczak, A. R., Quadri, R. F., Tran, K.-V. H., et al. 2014, ApJ, 783, 85
Tremonti, C. A., Heckman, T. M., Kauffmann, G., et al. 2004, ApJ, 613, 898
van de Voort, F., Schaye, J., Altay, G., & Theuns, T. 2012, MNRAS, 421, 2809
Williams, R. J., Quadri, R. F., Franx, M., van Dokkum, P., & Labbé, I. 2009, ApJ, 691, 1879
Yabe, K., Ohta, K., Iwamuro, F., et al. 2014, MNRAS, 437, 3647